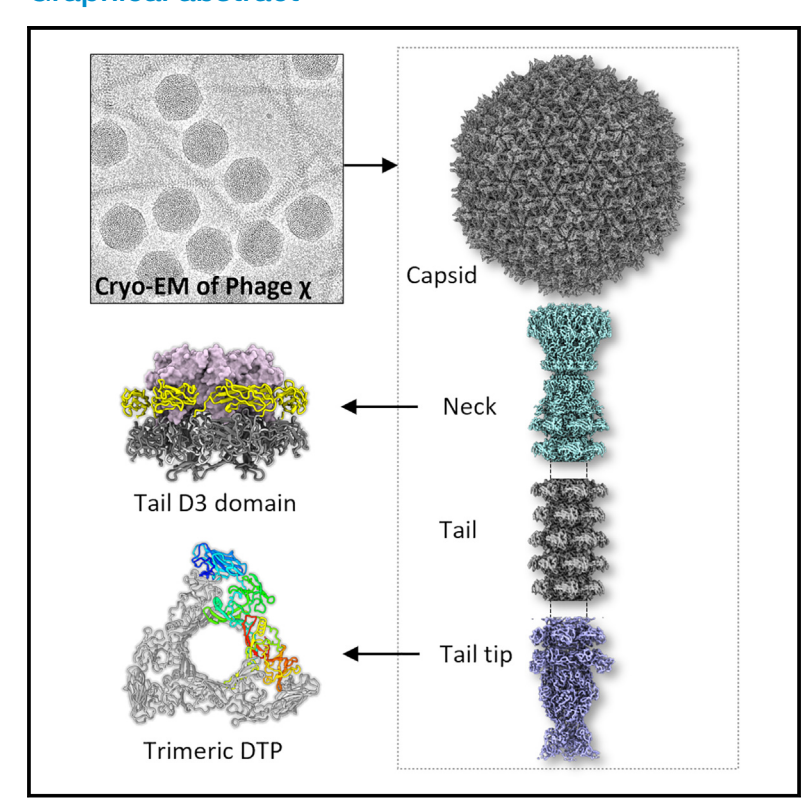
Structure

Cryo-EM structure of flagellotropic bacteriophage Chi

Graphical abstract



Authors

Ravi R. Sonani, Nathaniel C. Esteves, Birgit E. Scharf, Edward H. Egelman

Correspondence

bscharf@vt.edu (B.E.S.), egelman@virginia.edu (E.H.E.)

In brief

Sonani et al. report the structure of bacteriophage χ using cryo-EM, revealing its capsid, neck, tail, and tail-tip organization. Unique proteins in the neck and tail tip, including a trimeric assembly of distal tail protein, deviate from typical siphophage structures, shedding light on χ 's architecture and structural diversity among related bacteriophages.

Highlights

- Cryo-EM structures of bacteriophage χ 's neck and tail tip are solved
- Tail tube hexamer adopts a unique conformation at χ 's tailneck junction
- Trimeric distal tail protein reduces χ 's tail tip symmetry from 6-fold to 3-fold



Structure



Article

Cryo-EM structure of flagellotropic bacteriophage Chi

Ravi R. Sonani, 1 Nathaniel C. Esteves, 2 Birgit E. Scharf, 2,* and Edward H. Egelman1, 3,*

- ¹Department of Biochemistry and Molecular Genetics, University of Virginia School of Medicine, Charlottesville, VA 22903, USA
- ²Department of Biological Sciences, Virginia Tech, Blacksburg, VA 24061, USA

*Correspondence: bscharf@vt.edu (B.E.S.), egelman@virginia.edu (E.H.E.) https://doi.org/10.1016/j.str.2024.03.011

SUMMARY

The flagellotropic bacteriophage χ (Chi) infects bacteria via the flagellar filament. Despite years of study, its structural architecture remains partly characterized. Through cryo-EM, we unveil χ' s nearly complete structure, encompassing capsid, neck, tail, and tail tip. While the capsid and tail resemble phage YSD1, the neck and tail tip reveal new proteins and their arrangement. The neck shows a unique conformation of the tail tube protein, forming a socket-like structure for attachment to the neck. The tail tip comprises four proteins, including distal tail protein (DTP), two baseplate hub proteins (BH1P and BH2P), and tail tip assembly protein (TAP) exhibiting minimal organization compared to other siphophages. Deviating from the consensus in other siphophages, DTP in χ forms a trimeric assembly, reducing tail symmetry from 6-fold to 3-fold at the tip. These findings illuminate the previously unexplored structural organization of χ 's neck and tail tip.

INTRODUCTION

Bacteriophages (or phages) are regarded as promising candidates for diverse biotechnological applications due to their remarkable specificity toward host bacteria and intricate structural design. Phages recognize their host through receptor binding proteins (RBPs), which exhibit highly specific affinity for an extensive array of host surface epitopes such as membrane proteins, glycoproteins, and glycolipids. Detailed knowledge of the phage RBPs and their corresponding host receptors is crucial for a thorough understanding of phage infection biology and their potential applications in diagnostics and therapeutics.

Flagellotropic bacteriophages represent an intriguing phage category that exploits bacterial flagella as an initiation point for infection. This subset is characterized by the presence of tailor head-fibers that encase the bacterial flagellum. Bacteriophage Chi (χ), a member of this specialized group initially characterized in the 1930s and further examined in the 1960s, Pelies on the recognition of the flagellar filament for successful infection. It belongs to the *Siphoviridae* family, comprising non-contractile-tail-containing double-stranded DNA bacteriophages. Delectron microscopic studies of χ demonstrate the presence of a thin tail fiber attached to the phage tail tip that wraps around the bacterial flagellar filament, establishing the initial contact. L11,12

Phage χ has garnered attention due to the discovery of other χ -like bacteriophages ^{13–16} and their ability to infect potential pathogenic bacteria such as *Escherichia coli*, *Salmonella*, *Serratia*, *Enterobacter cancerogenous*, ¹⁵ and *Providencia stuartii*. ¹⁶ In 2013, the genome of χ , consisting of 75

open reading frames, was sequenced. 17,18 However, the identification of corresponding χ proteins remained elusive until 2019, when tail proteins gp22, gp25, and gp29 were recognized through immunogold labeling in the χ homolog YSD1. 14 More recently, cryo-electron microscopy (cryo-EM) of the *Salmonella typhi*-specific YSD1 revealed that gp16 and gp17 are forming the capsid, and confirmed that gp22 is the major tail protein. 19 This study provided a detailed description of the molecular structure of the capsid and tail, specifically elucidating the structural features responsible for phage stability. 19 However, structures of the tail-tip, which serves as attachment of the tail fiber, and the neck, where the capsid joins the tail, remained elusive.

We employed cryo-EM to elucidate the structural details of the capsid, neck (capsid-tail junction), tail, and tail-tip of bacteriophage χ . The cryo-EM analysis revealed that the capsid and tail structures closely resemble those observed for YSD1. However, the neck and tail-tip structures revealed previously unidentified proteins in the architectural composition of χ . The structural analysis of the neck disclosed that the tail tube protein gp22 adopts the different conformation in the neck-proximal tail hexamer, forming a socket-like structure for the attachment of the neck. Unlike other siphophages, the χ tail tip is a minimal protein complex composed of only four different protein species. Notably, the distal tail protein (DTP) in χ is a trimeric assembly, facilitating the reduction of tail-to-tip symmetry from C6 to C3. This finding is in contrast with the hexameric DTP observed in other siphophage tail tip structures. 20-22 Our structural analysis suggests that BH2P likely constitutes the proximal part of the tail fiber.

³Lead contact





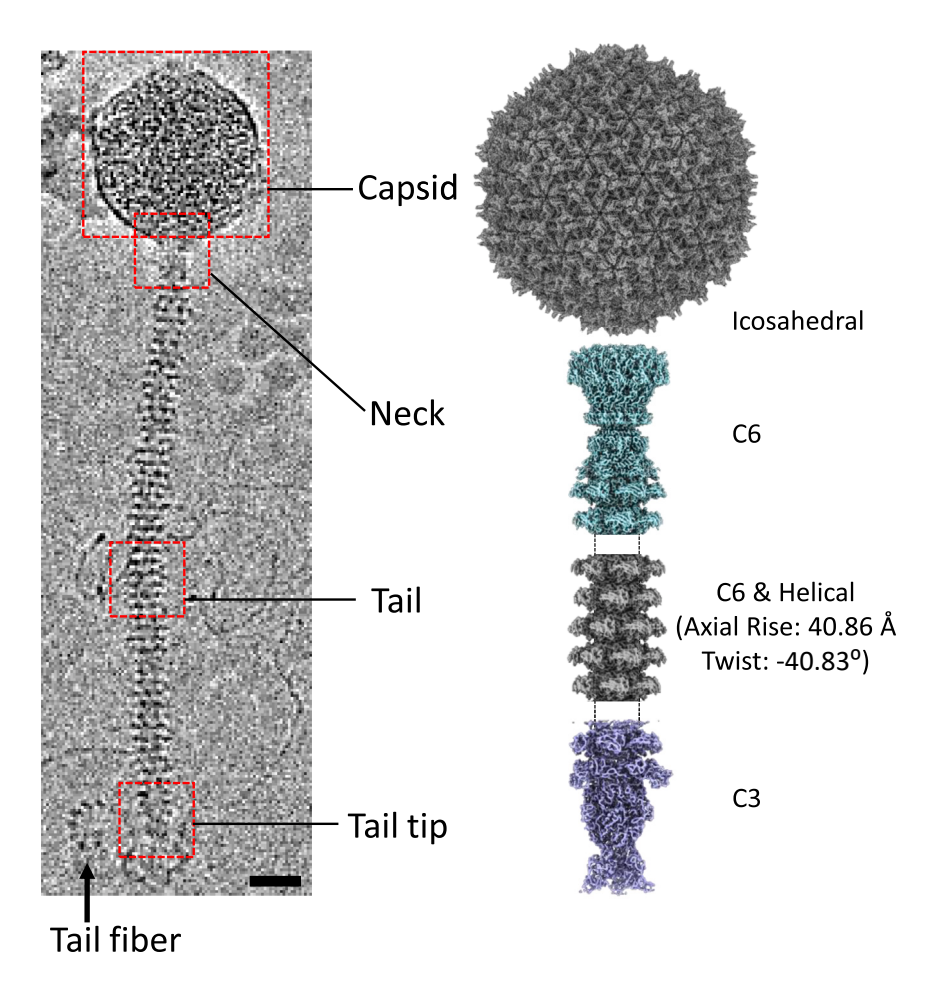


Figure 1. Cryo-EM reconstructions of different substructures of bacteriophage χ Capsid, neck, tail, and tail tip are reconstructed by imposing different symmetries. Scale bar, 20 nm.

Neck architecture of χ

The neck architecture involves the placement of the uppermost dodecameric portal ring (12 \times gp14) within the 5-fold vertex of the capsid, referred to as the portal vertex. The dodecameric neck 1 ring (12 x gp13), also recognized as the head completion ring, associates with the portal ring. This is followed by the assembly of the hexameric neck 2 ring (6 × gp19), serving as the head-to-tail connector ring, and the hexameric tail terminator (6 x gp21). The neck is ultimately linked to the neck-proximal hexamer of the tail (6 \times gp22) (Figure 2). The anti-parallel β sheets of neck 1, neck 2, and tail terminator protein form a continuous barrel smoothly extending the portal lumen to the tail tube.

The portal subunit and its assembly in χ exhibit a typical structure similar to that observed in the necks of myo- $^{23-25}$ and siphophages^{22,26,27} and devoid of barrel-like extension as observed for podophages.²⁸ Like classic T4 portal, the portal in X is comprised of distinct domains,

namely the crown, wing, stem, and clip, forming the topmost, middle, lower middle, and lower part of the portal assembly, respectively (Figure S2). In contrast, the neck 1 protein in χ , with its compact size of 84 residues, diverges significantly from the structures reported in other siphophages. 22,26,27 Neck 1 consists of two α -helices connected by two anti-parallel β -strands, and a C-terminal strand (Figure 3A). The C-terminal strand engages with the clip domain of the portal ring, contributing to the stabilization of the neck structure (Figure 3A). Two helices orient outward from the lumen of the neck, forming a structural platform for the secure attachment of the neck into the portal vertex of the capsid. The antiparallel β sheet is oriented in the neck lumen parallel to the central axis (Figure 3A). Notably, its luminal (positively charged) and outer (negatively charged) surfaces display opposite charges, attributed to the presence of basic residues (R31 and R40) and acidic residues (D35 and E39), respectively (Figure 3A). This arrangement of the 12 β sheets creates an adapter ring with an approximate diameter of ~30 Å, featuring a positively charged lumen that likely anchors the negatively charged DNA. The negatively charged outer rim of the adapter ring fits into the positively charged socket of neck 2 (gp19), formed by the N-terminal helix (residues 1-20) of gp19 (Figure 3A).

Beneath neck 1, both neck 2 and the tail terminator exhibit structural similarities to those observed in other siphophages, namely *Roseobacter*, ²⁷ DT57C, ²² and SPP1, ²⁶ at both the subunit and

RESULTS

Cryo-EM reconstructions and overall structure of phage γ

We reconstructed the capsid, neck (capsid-tail junction), tail, and tail-tip structures of bacteriophage χ by applying icosahedral, C6, helical (with a rise/twist of 40.86 Å/-40.83° along with C6 symmetry), and C3 symmetry, respectively (Figure 1). The high quality of these maps facilitated *de novo* model building for all regions, leading to the identification of a total of 12 structural proteins (Table 1). The structural analysis revealed a similarity between the χ capsid and tail structures and those of bacteriophage YSD1 as expected due to high sequence identities ¹⁹(Figure S1).

The χ tail tube protein (gp22) is comprised of three domains that are rich in β strands: D1 (residues 1–97, 201–276), forming the core of the tail tube; D2 (residues 98–200), forming the outer wall of the tail; and D3 (residues 277–381), extending outward from the tail surface. The relative orientation of D3 is fixed in the neck but not over the majority of the tail structure. The capsid is composed of two proteins, the major capsid protein (gp17) and the auxiliary protein (gp16) as observed in the capsid of phage YSD1 (Figure S1).

As certain structures are very similar to the ones reported for the related phage YSD1, the emphasis of this study lies in the description of neck and tail-tip structures of phage χ , revealing distinctive features in their structural composition.

Structure Article



Table 1. Structural annotation of phage χ proteins

Substructure	Protein Uniprot ID	Structural Annotation	Length (AAs)
Capsid	M9NUS8 (gp17)	Major capsid protein	354
	M9NSZ8 (gp16)	Auxiliary capsid protein	139
Neck	M9NUF0 (gp14)	Portal	560
	M9NTK8 (gp13)	Neck 1	84
	M9NUF1 (gp19)	Neck 2	121
	M9NT01 (gp21)	Tail terminator	167
Tail	M9NUS9 (gp22)	Tail tube protein	381
Tail tip	M9NT03 (gp26)	Distal tail protein	562
	M9NTL4 (gp28)	Tail tip assembly protein	76
	M9NUT0 (gp27)	Baseplate hub 1 protein	272
	M9NVD3 (gp30)	Baseplate hub 2 protein	1296
	M9NVD0 (gp25)	Tape measure potein	1431

oligomeric levels (Figure S2). In addition to providing a docking site for neck 1, neck 2 predominantly adopts a β - strand structure, featuring the tail tube protein (TTP)-like domain that seamlessly extends the neck lumen from neck 1 to the tail terminator. Additionally, neck 2 includes an anti-parallel β sheet (residues 43–64) that is positioned in the neck lumen, akin to the structural arrangement observed in neck 1. The presence of the positively charged residue K45 on this loop suggests a potential role in DNA anchoring, similar to the function attributed to neck 1. In contrast, the tail terminator presents a mixed structure composed of α helices and β sheet elements, establishing a connection of the neck to the neck-proximal tail hexamer (Figure S2).

The interaction between the χ tail terminator and neck-proximal tail hexamer is peculiar (Figure 3B). In the C6 symmetrized map of the neck, the density for the D3 domain of neck-proximal tail hexamer, which is typically disordered along the length of the tail, is resolved. The D3 domain is predominantly composed of β strands and assumes the structural features of a bacterial Ig-like domain 1 (Big-1), as previously postulated. ¹⁹ It is positioned atop the D2 domain of the adjacent subunit, thereby creating an additional outer hexameric ring referred to as the D3 ring, situated above the D2 ring (Figure 3B).

Previously, the D3 domain of the YSD1 phage tail, which has an over 99% sequence identity with the D3 domain of χ , was hypothesized to lack a structural function but instead to have a role in phage-host binding. ¹⁹ In contrast, the D3 domains of the top tail ring in χ form a socket-like module facilitating the docking of the tail terminator.

The tail tip of χ exhibits minimal complexity

Unlike other siphophages, ^{20–22} the tail tip exhibits a minimalistic arrangement. It is comprised of four proteins—distal tip protein (DTP, gp26), baseplate hub 1 protein (BH1P, gp27), baseplate hub 2 protein (BH2P, gp30), and tail assembly protein (TAP, gp28) (Figure 4). The DTP trimer serves as a structural link be-

tween the hexameric tail and the trimeric tail tip. BH1P and BH2P interact directly with DTP, forming the proximal and distal components of the tail tip, respectively. The core of the tail tip is filled by both TAP and the C-terminal residues 1400–1431 of the tape measure protein (TMP, gp25). The C-terminal region of TAP extends further into BH2P, contributing to the intricate interweaving of the tail-tip assembly. The absence of visible density for the C-terminal residues 771–1296 of BH2P indicates its uncertain position relative to the tail tip. Furthermore, the structural organization of BH2P implies that its residues 771–1296 are likely to form the proximal part of the tail fiber.

The elongated structure of DTP reduces the C6 symmetry of the tail to the C3 symmetry of the tail tip

The DTP is a protein composed of 562 residues, primarily adopting a β-strand structure characterized by two distinct domains: the N-terminal domain (DTP_{NTD}, residues 1–150) forming a jelly roll fold, and the C-terminal domain (DTP_{CTD}, residues 151-562) forming an extended β-sandwich domain reminiscent of the fused D1 domains of two TTPs¹⁹ (Figure 5A). The trimeric assembly of DTP plays a crucial role in connecting the C6 symmetrical tail tube to the C3 symmetrical tail tip (Figures 5B and 5C). While DTP_{CTD} facilitates the oligomerization of the DTP assembly and enables the smooth extension of the tail tube to the tail tip, DTP_{NTD} protrudes from the tail wall, forming a triangular baseplate-like structure (Figures 5A and 5B). Foldseek analysis of DTP_{NTD} suggests its structural similarity with the galactose-binding domain-like superfamily. The extended surface of DTP_{CTD} interacts with two TTPs, where the loops of the TTPs (TTP₄₇₋₆₈) containing residues 47-68 sit in two pockets of DTP_{CTD} (Figure 5B). The TTP₄₇₋₆₈ loops are polar at the tip, fitting into the polar region of the pocket on DTP_{CTD} and possess a small, non-polar patch interacting with the non-polar linings of the pocket on DTP_{CTD} (Figure 5C). The interaction of six TTP₄₇₋₆₈ loops with three DTPs results in a total interfacial area of approximately 3,840 Å², averaging around 640 Å² per loop.

Moving downward, DTP_{CTD} provides a surface for the interaction with BH1P and BH2P. Remarkably, the interactions between DTP and BHPs are predominantly electrostatic, with an interfacial area of approximately 1,330 Å² and 880 Å² for BH1P and BH2P, respectively (Figure 5C). Two loops (loop 1: residues 177-196; and loop 2: residues 377-394) and the very C-terminal strand (residues 552-562) of DTP_{CTD} form a ring at the bottom rim of the DTP trimer, providing a surface for the attachment of BH1P and BH2P. This ring exhibits alternating positively and negatively charged bands, forming the binding sites for BHPs (Figure 5B). The binding site of BH1P is situated at the interface of two DTP subunits formed by loop 1 and loop 2 of neighboring subunits (Figures 5B and 5C). Conversely, the BH2P binding site is formed by loop 1 and the C-terminal strand of a single DTP (Figures 5B and 5C). Both BHP binding sites share a similar electrostatic nature, displaying a half-negative and half-positive charge distribution (Figures 5B and 5C). In summary, while each DTP_{CTD} bridges two TTPs with a pair of BHPs, the DTP_{NTD} protrudes outward, forming a baseplate-like structure.

BH1P and BH2P form the tail tip

BH1P (272 residues) and BH2P (1296 residues) are multidomain proteins constituting the tail tip (Figure 6). Intriguingly, BH1P



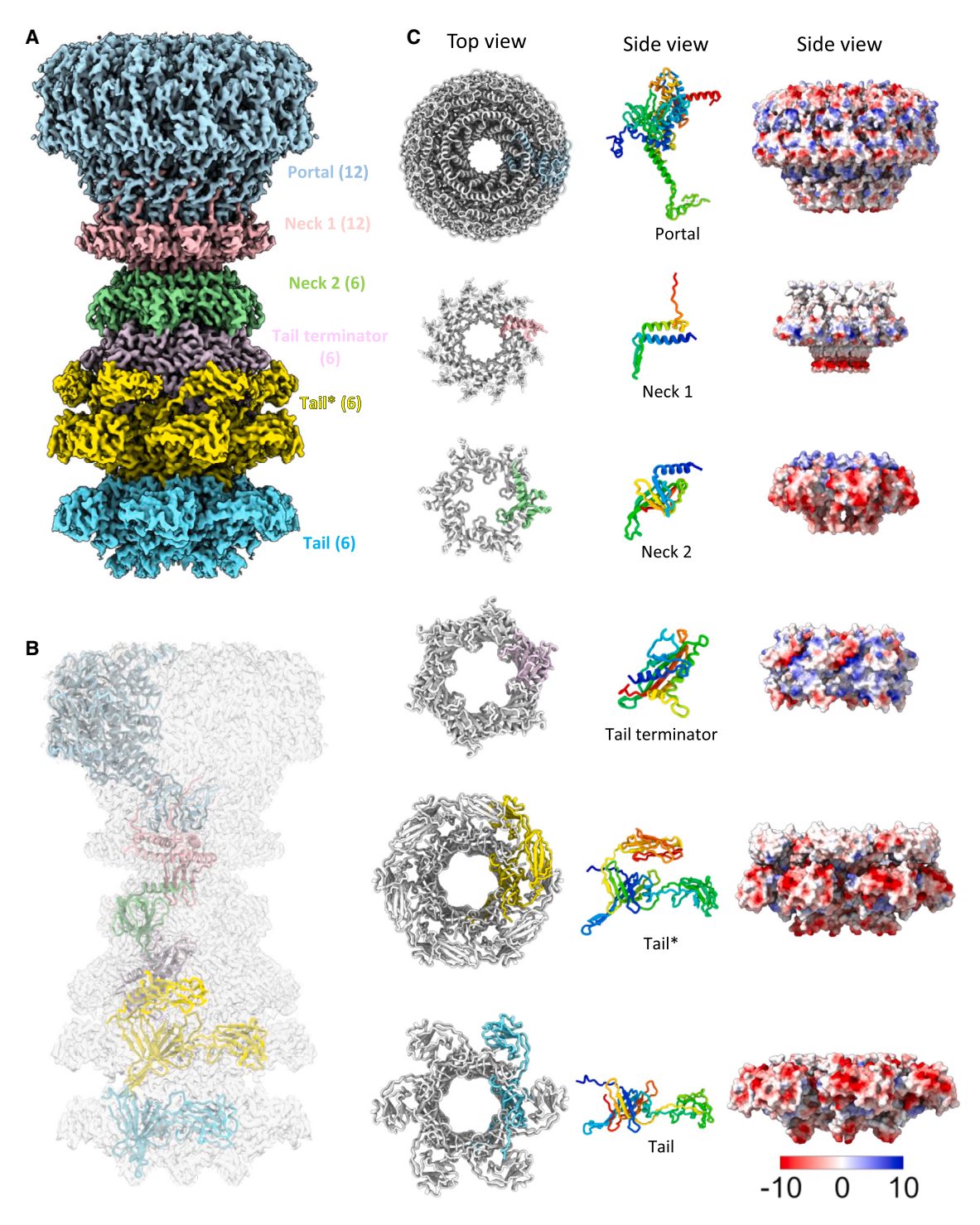


Figure 2. Structure of χ neck

(A) Cryo-EM density map of neck.

(B) Cryo-EM map fitted with neck asymmetric unit.

(C) Top and side view of different parts of the neck. The left, middle, and right columns show oligomer, monomer (N- to C-terminal colored blue to red), and surface (colored by electrostatics).

shares homology with the hub proteins of Dinoroseobacter phage vB_DshS-R4C²⁷ (gp14) and Rhodobacter GTP (RCAP_ rcc01696),²⁹ displaying approximately 23% sequence identity. BH1P is comprised of four domains: attachment (residues 1-139), metal binding (residues 140-159, 237-259), carbohydrate binding (residues 160-236), and clip (residues 260-272)

Structure Article



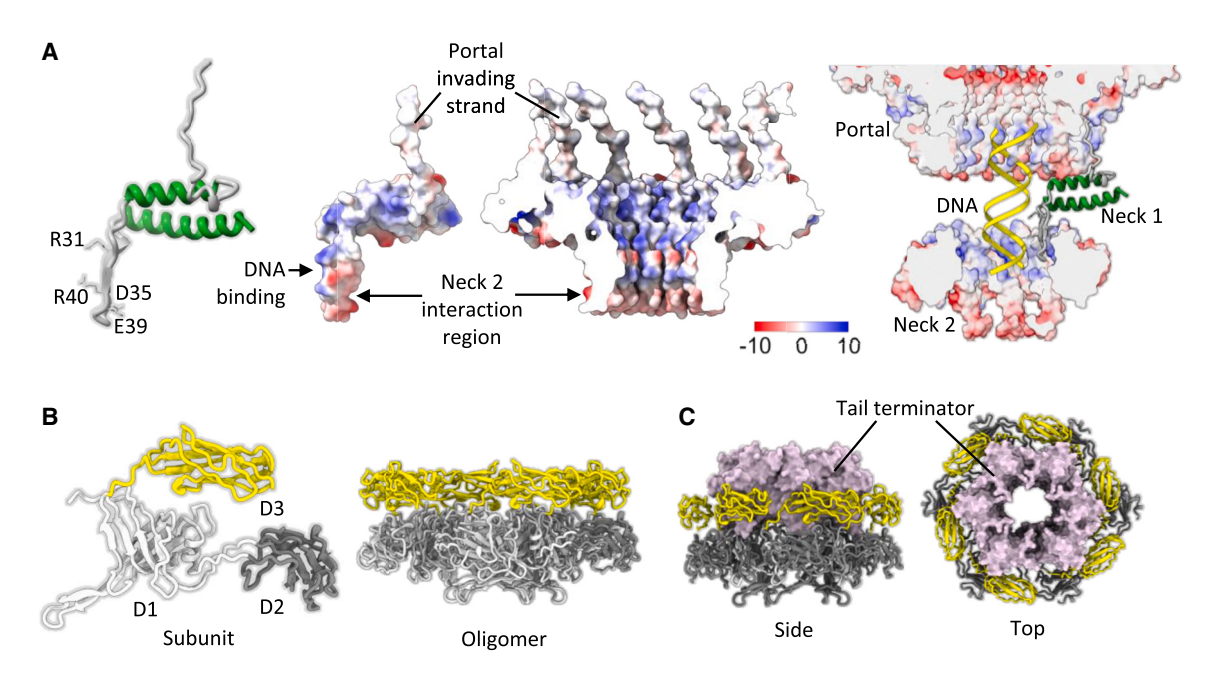


Figure 3. Structure of neck 1 and neck-proximal tail tube protein

(A) From left to right: Structure of neck 1 monomer colored by secondary structural elements, surface view of subunit and oligomer colored by electrostatics, and neck 1 subunit interacting with portal, DNA, and neck 2.

- (B) Structure of neck-proximal tail tube protein subunit and oligomer colored by its D1,D2, and D3 domains.
- (C) Side and top view of the socket formed by D3 domains of neck-proximal tail tube hexamer forming the socket for tail-terminator to dock in.

(Figures 6B, 6C, and 6D). The arrangement of BH1P domains in the tail tip proceeds from top to bottom, with the topmost attachment domain binding to the DTP ring, followed by the carbohydrate binding domain forming the upper region of the tail tip, and the metal-binding domain and clip forming the middle region of the tail tip (Figure 6B). Notably, the clip in χ BH1P is shorter compared to that in vB_DshS-R4C 27 and GTP. 29

While the density for the entire BH1P is apparent, the density for residues 771-1296 of BH2P is not visible, possibly due to its positional disorder (Figure 4). The structure of BH2P (residues 1-770) exhibits partial similarity to the E. coli phage T5 hub protein pb3²¹ and phage lambda hub protein gpJ,²⁰ despite the absence of sequence similarities (Figure S3). BH2P consists of two modules: the tail-tip module (residues 1-396) and the tip extension module (residues 416-770), connected by a linker 1 (residues 396-415) (Figures 6A, 6C, and 6D). The tail-tip module is comprised of four domains: tip (residues 1-130), upper tip I (residue 131-245), attachment (residues 246-270, 338-395), and upper tip II (residues 271-337), forming the tail tip (Figures 6A, 6C, and 6D). The polarity of BH2P in the tail tip is reversed compared to BH1P, with the first, N-terminal tip domain forming the very end of the tail tip. It runs upwards, followed by upper tip I, attachment, and upper tip II domains, forming the upper tip (Figures 6A, 6C, and 6D). The tip extension module is comprised of two domains: tip extension (residues 416-625) and Ig-like I (residues 626-770), extending the tip for tail fiber attachment (Figures 6A, 6C, and 6D).

Several domains of BH1P and BH2P exhibit a TTP-like fold, commonly referred to as hub domains (HDI, HDII, HDIII, HDIV, and so on).^{21,30} Hence, the attachment and carbohydrate bind-

ing domains of BH1P are equivalent to HDI and HDII domains, respectively (Figure 6B). Similarly, the tip and attachment domains of BH2P are equivalent to the HDIII and HDIV domains, respectively (Figure 6A). In summary, the tail tip is formed by BH1P and BH2P, while the tip extension region is exclusively formed by BH2P (Figure 6D). Anti-parallel β sheets of the attachment domain of BH1P (HDI) and BH2P (HDIV) form the barrel akin to the hexameric tail tube, which binds to the DTP ring and extends the tail lumen (Figure 6D). The upper tip domains of BH2P form the upper region of the tail tip, while the carbohydrate binding domain of BH1P further decorates it (Figure 6D). The metal-binding and clip domains of BH1P and the tip domain of BH2P form the very tip region (Figure 6D). Lastly, the tip extension module of BH2P extends the tail tip toward the tail fiber (Figure 6D).

The χ tail tip possesses the C-terminal helical domain (residues 1400–1430) of TMP housed within the tail proximal part of the tip lumen as also observed in the tail tips of bacteriophages T5, 21 lambda, 20 80 α , 31 and DT57C. 22 Three such TMP subunits form the 3-fold coiled-coil of α helices (Figures 4C and 6E). Notably, the additional density underneath the TMP reveals the presence of a small 76-residue protein, a tail tip assembly protein (Figures 6E and 6F). Structurally, TAP consists only of one α helix (residues 1–12), followed by a flexible C-terminal strand. The TAP helix is positioned beneath the TMP trimer, sealing the space between TMP and the tail tip. A portion of the C-terminal strand (residues 13–49) does not follow the C3 symmetry, as its density is not visible. However, its remaining 3-fold part (residues 50–76) is apparent in the map, intruding into the tip domain of BH2P, further stabilizing the tail tip complex (Figures 6E and 6F).



Structure Article

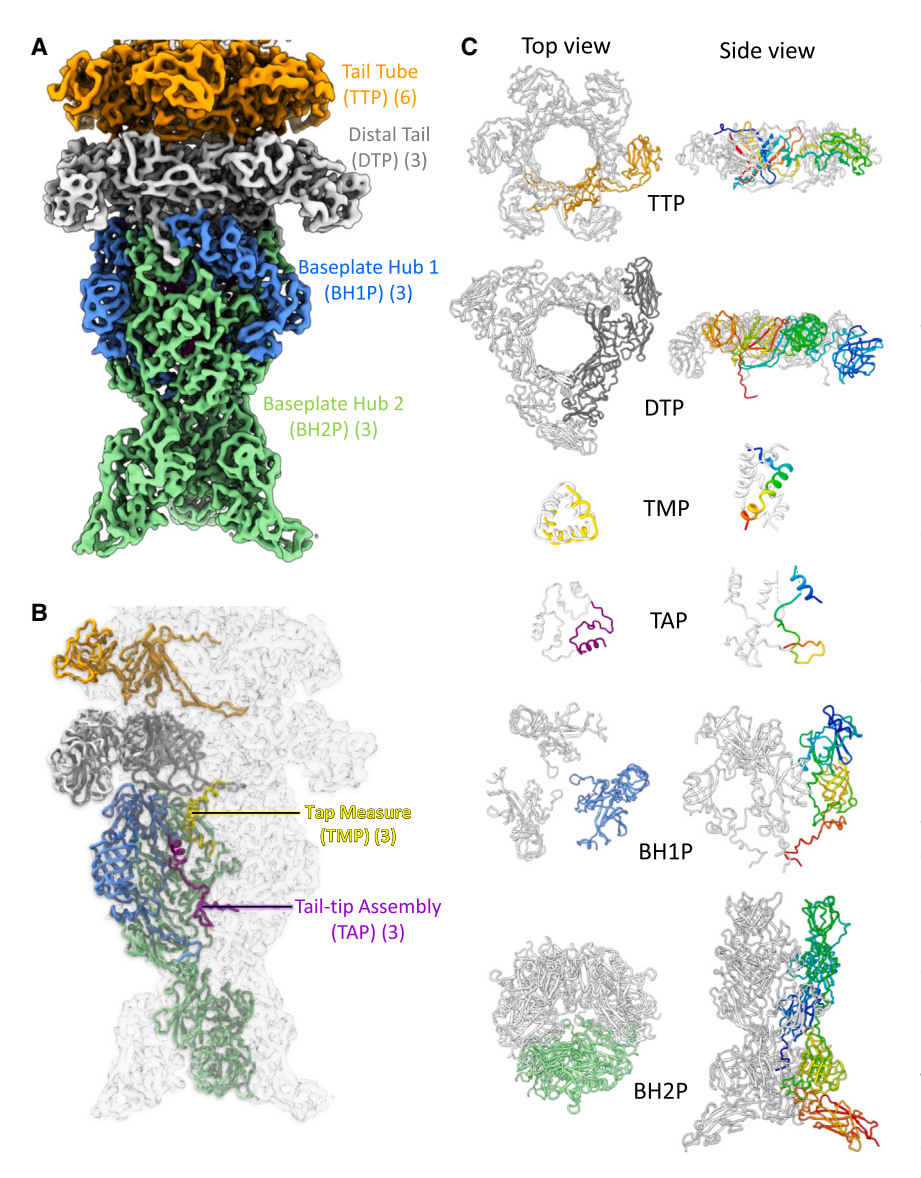


Figure 4. Structure of tail tip

(A) Cryo-EM density map of tail tip. (B) Cryo-EM map fitted with tail tip asymmetric unit. (C) Top and side view of different parts of tail tip. N- to C-terminal domains of subunits in the right column are colored blue to red.

its β strands, imparting a positive charge and rendering it suitable for DNA binding. The structural similarities and the conservation of arginine residues in both proteins suggest a potential role for neck 1 in DNA anchoring. Second, the D3 domain conformation of the neck-proximal tail hexamer differs from the rest of the tail. establishing a socket-like structure for the docking of the neck. The D3 domain of the YSD1 phage tail protein (YSD1_ 22), which shares over 99% sequence identity with χ, was previously hypothesized to lack a structural role but instead to be involved in phage-host binding.19 In contrast, our findings suggest that the D3 domains of the neck-proximal tail hexamer significantly contribute to the interaction between the tail and tail terminator. This contribution results in an increased tail-tail terminator interface to approximately 8,280 Å2, compared to an expected \sim 5,390 $\mbox{Å}^2$ in the absence of the ordered D3 domain. This finding implies that the D3 domains of the neck-proximal hexamer, unlike the other tail hexamers, play a crucial role in stabilizing the neck iunction.

The fully assembled capsid and tail are glued together through the neck region in the phage assembly process. Based on the neck structure of χ , the anticipated

steps in phage assembly are as follows. Neck 1 binds to the portal ring to seal the capsid at the portal side, whereas tail terminator attaches and terminates the tail assembly. The flexible D3 domain of the top tail hexamer is likely to adopt a C6-fold orientation forming the socket-like structure during tail-terminator attachment. Finally, neck 2 acts as a glue between neck 1 (sealed capsid) and tail terminator, forming a stable connection. It is worth noting that the electrostatic potential of neck 2 and the tail terminator lumen is negatively charged, differing from neck 1 and suggesting a role in facilitating DNA conduits.

The tail tip structure of χ is minimalistic as compared to the complex tail tips of bacteriophages T5²¹ and DT57C.²² It is comprised of four proteins: DTP, TAP, BH1P, and BH2P. In previously reported siphophage tail-tip structures, ^{20–22} the reduction from tail (C6) to tip (C3) symmetry is consistently attributed to the adjustment by the hub domains of the BHPs. The typical architecture involves the tail-tube hexamer ending with the DTP hexamer, connected to the hub domains of the BHPs. However, the χ tail tip deviates from this consensus, as its elongated

DISCUSSION

The cryo-electron microscopy (cryo-EM) analysis of bacterio-phage χ reveals the presence of a total of 12 proteins in its structural composition, distributed among the neck, tail tip, capsid, and tail (Table 1). While several of these proteins have been previously identified in the χ homolog YSD1 using cryo-EM¹⁹ and molecular biology techniques, ¹⁴ the present study identifies previously unknown proteins, including tail tip assembly protein (TAP), baseplate hub 1 protein (BH1P), and neck 1. Our cryo-EM structures offer insights into their potential physiological functions.

The neck of χ exhibits two structural features that distinguish it from the neck of other siphophages. First, the neck 1 protein is notably smaller than its counterparts in other siphophages. ^{22,26,27} A Foldseek search for neck 1 reveals a structural homolog in the head completion protein of the lambda phage (PDB id: 8K38; Uniprot id: P68660). The invasion pattern of neck 1 into the lambda phage portal is similar to that observed in χ neck 1. Additionally, lambda neck 1 contains two arginine residues on

Structure Article



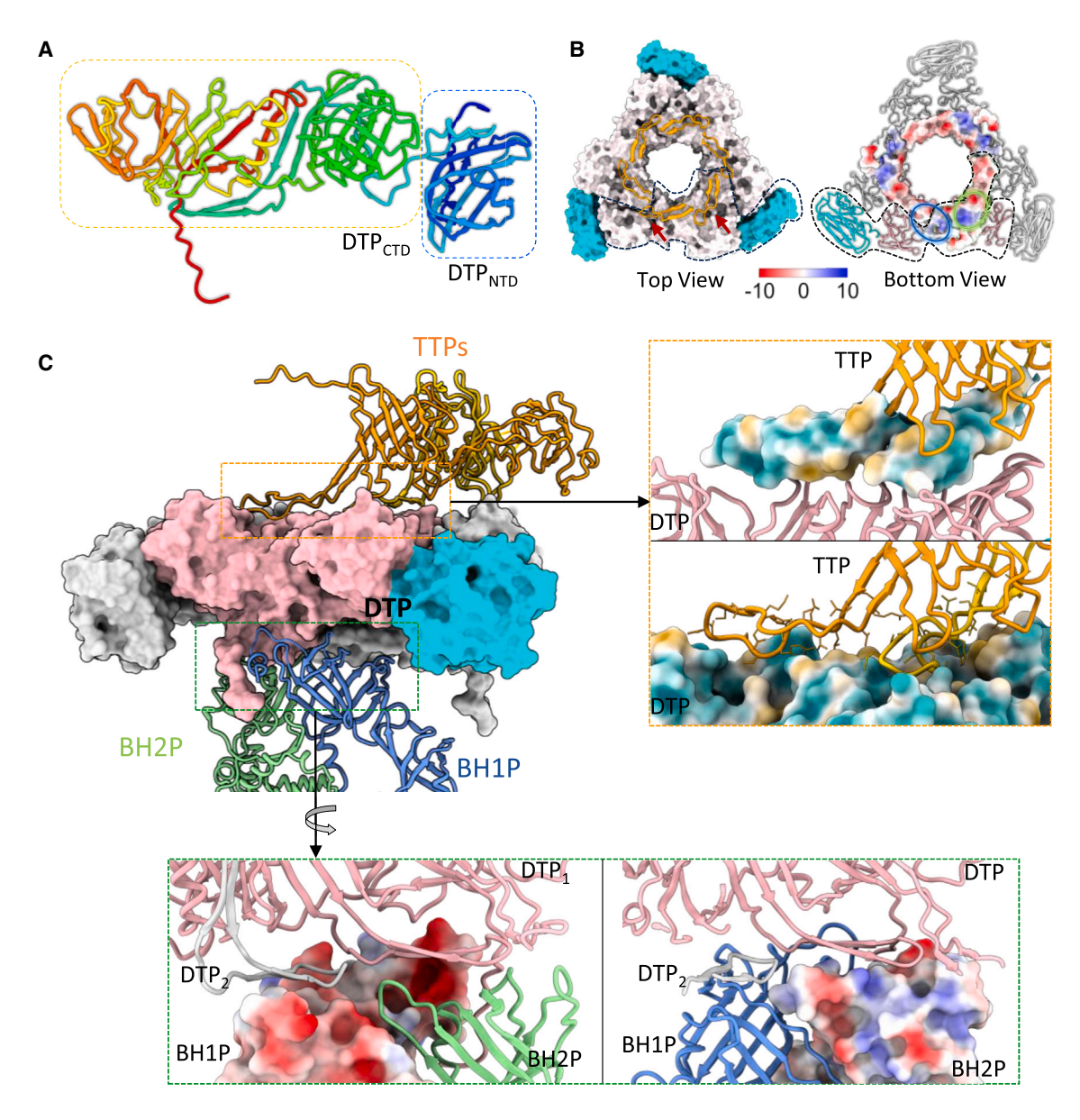


Figure 5. Distal tail protein (DTP) joins tail to tail tip

(A) Structure of DTP depicting its two domains, DTP_{NTD} and DTP_{CTD} . N- to C-terminal domains are colored blue to red.

(B) Top and bottom view of DTP trimer showing binding sites for tail tube protein (TTP) (red arrows) and baseplate hub proteins (BHPs – BH1P and BH2P) (blue and green circles), respectively.

(C) Interaction of DTP trimer with TTP, BH1P, and BH2P. Close-up views of DTP-TTP and DTP-BHPs interactions are shown in right and lower panel, respectively.

DTP forms a trimer instead of a hexamer at the tail end, mediating the symmetry reduction from tail to tip.

The structural analysis reveals that TAP and TMP primarily serve a structural role, as they lack surface accessibility in the χ tail tip. Since these both proteins form the core of the tail tip, their rearrangement is necessary for dismantling of tail tip and subsequent DNA release. Conversely, DTP, BH1P, and BH2P are likely to play roles in both, the structural framework and phage-host interactions. The presence of carbohydrate-binding domains in DTP and BH1P, along with the Ig-like domain in BH2P, suggests their potential involvement in binding to the host surface.

The density for the C-terminal region of BH2P with residues 771–1296 is not visible in our map, likely indicating its role in forming the proximal part of the tail fiber. The AlphaFold-predicted structure of this region shows four structural domains: linker 2 (residues 771–845), Ig-like II domain (residues 846–1035), Ig-like III domain (residues 1036–1200), and C-terminal tail (residues 1201–1296) (Figure S4). The presence of a potentially flexible linker 2 between the tip extension module and Iglike II domain explains why BH2P residues 771–1296 exhibit no fixed conformation relative to the tail tip. The presence of two additional Ig-like domains in the C-terminal region of BH2P suggests its potential role in host binding.





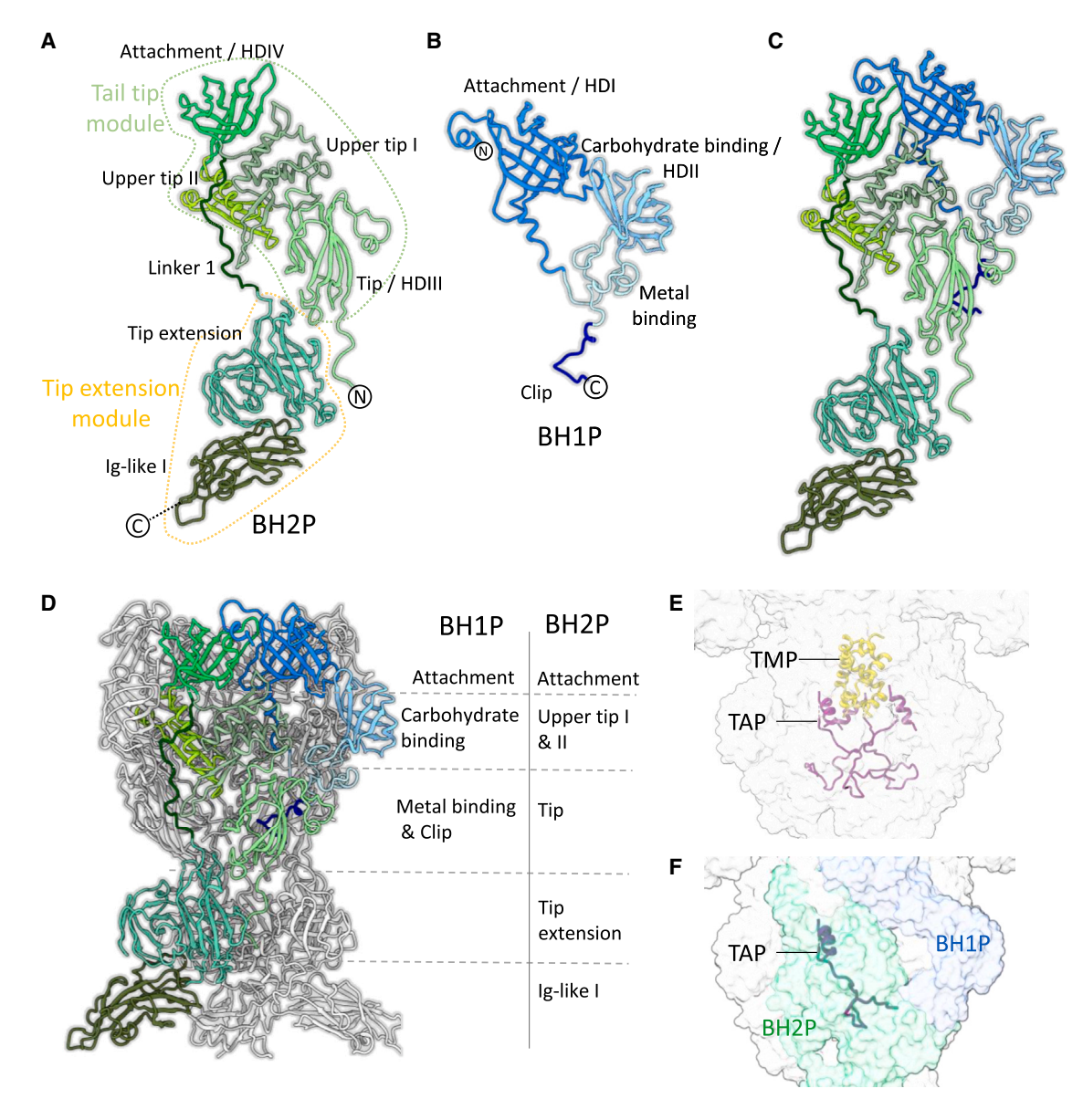


Figure 6. Base hub proteins (BHPs) forming tail tip

Structural domains of (A) BH1P, (B) BH2P, and (C) their visualization in BH1P-BH2P complex. (D) Location of BH1P and BH2P domains in tail tip structure. (E) Tail assembly protein (TAP) and tape measure proteins (TMP), housed in the lumen of the tail tip.

STAR*METHODS

Detailed methods are provided in the online version of this paper and include the following:

- KEY RESOURCES TABLE
- RESOURCE AVAILABILITY
 - Lead contact
 - Materials availability
 - O Data and code availability
- EXPERIMENTAL MODEL AND STUDY PARTICIPANT DETAILS
 - \circ Growth conditions for bacteria and phage χ
- METHOD DETAILS

- \circ Cultivation and purification of χ particles
- O Cryo-electron microscopy
- Model building
- O Structural analysis
- QUANTIFICATION AND STATISTICAL ANALYSIS

SUPPLEMENTAL INFORMATION

Supplemental information can be found online at https://doi.org/10.1016/j.str. 2024.03.011.

ACKNOWLEDGMENTS

E.H.E. was funded by NIH grant GM122510. B.E.S. was funded by NSF grant IOS-2054392. We thank Tomek Osinski for computational support. Electron

Structure Article



Table 2. Cryo-EM data collection and refinement statistics of capsid, neck, tail, and tail tip structures of bacteriophage χ				
	Neck	Tail tip	Tail	Capsid
PDB entry	8VHX	8VJH	8VJA	8VJI
EMBD entry	43243	43281	43278	43282
Voltage (kV)	300	300	300	300
Magnification (x)	105,000	105,000	105,000	105,000
Electron exposure (e ⁻ /Å ²)	50	50	50	50
Pixel size (Å/pixel)	0.82	0.82	0.82	1.0677
Particle images (no.)	17,766	2,159	83,657	28,512
Symmetry imposed				
	Point group: C6	Point group: C3	Helical Rise: 40.86 Å Twist: –40.83° Point group: C6	Icosahedral
Map global resolution (Å)		·	·	
Map:map Fourier shell correlation (FSC, 0.143)	2.9 Å	4.2 Å	2.7 Å	3.3 Å
Model:map FSC (0.5)	3.1 Å	4.2 Å	3.1 Å	3.5 Å
Refinement and model validation				
Residues	2060	2219	275	3318
Clash score	4.22	10.00	0.97	8.47
R.M.D deviations				
Bond length (Å)	0.013	0.002	0.011	0.009
Bond angle (°)	0.731	0.594	1.77	0.823
Ramachandran plot (%)				
Outliers	0.00	0.00	0.00	0.00
Allowed	2.70	7.90	2.56	5.74
Favored	97.30	92.10	97.44	94.26
Model vs. Data fit				
CC (mask)	0.86	0.72	0.82	0.85
CC (volume)	0.81	0.72	0.81	0.85

Microscopy was performed at the University of Virginia Molecular Electron Microscopy Core facility.

AUTHOR CONTRIBUTIONS

E.H.E., B.E.S., and R.R.S. conceptualized the project. R.R.S. performed the cryo-EM experiment, data processing, and structural analysis. N.C.E. prepared the sample. R.R.S., E.H.E., and B.E.S. wrote the paper.

DECLARATION OF INTERESTS

The authors declare no competing interest.

Received: January 7, 2024 Revised: February 8, 2024 Accepted: March 19, 2024 Published: April 12, 2024

REFERENCES

 Santos, S.B., Costa, A.R., Carvalho, C., Nóbrega, F.L., and Azeredo, J. (2018). Exploiting bacteriophage proteomes: the hidden biotechnological potential. Trends Biotechnol. 36, 966–984.

- Harada, L.K., Silva, E.C., Campos, W.F., Del Fiol, F.S., Vila, M., Dabrowska, K., Krylov, V.N., and Balcão, V.M. (2018). Biotechnological applications of bacteriophages: State of the art. Microbiol. Res. 212– 213, 38–58.
- Haq, I.U., Chaudhry, W.N., Akhtar, M.N., Andleeb, S., and Qadri, I. (2012).
 Bacteriophages and their implications on future biotechnology: a review.
 Virol. J. 9. 1–8.
- Dowah, A.S.A., and Clokie, M.R.J. (2018). Review of the nature, diversity and structure of bacteriophage receptor binding proteins that target Gram-positive bacteria. Biophys. Rev. 10, 535–542.
- Klumpp, J., Dunne, M., and Loessner, M.J. (2023). A perfect fit: Bacteriophage receptor-binding proteins for diagnostic and therapeutic applications. Curr. Opin. Microbiol. 71, 102240.
- Esteves, N.C., and Scharf, B.E. (2022). Flagellotropic Bacteriophages: Opportunities and Challenges for Antimicrobial Applications. Int. J. Mol. Sci. 23, 7084.
- Sertic, V., and Boulgakov, N. (1936). Bactériophages spécifiques pour des variétés bactériennes flagellées. Comptes Rendus Seances Soc. Biol. Ses Fil. 123, 887–888.
- lino, T., and Mitani, M. (1967). Infection of Serratia marcescens by bacteriophage chi. J. Virol. 1, 445–447. https://doi.org/10.1128/jvi.1.2.445-447.1967.



Structure Article

- Sword, C., and Pickett, M. (1961). The isolation and characterization of bacteriophages from Listeria monocytogenes. Microbiology 25, 241–248.
- Adriaenssens, E.M., Sullivan, M.B., Knezevic, P., van Zyl, L.J., Sarkar, B.L., Dutilh, B.E., Alfenas-Zerbini, P., Łobocka, M., Tong, Y., Brister, J.R., et al. (2020). Taxonomy of prokaryotic viruses: 2018-2019 update from the ICTV Bacterial and Archaeal Viruses Subcommittee. Arch. Virol. 165, 1253–1260.
- Icho, T., and lino, T. (1978). Isolation and characterization of motile *Escherichia coli* mutants resistant to bacteriophage chi. J. Bacteriol. 134, 854–860.
- Ravid, S., and Eisenbach, M. (1983). Correlation between bacteriophage chi adsorption and mode of flagellar rotation of *Escherichia coli* chemotaxis mutants. J. Bacteriol. 154, 604–611.
- Cobbley, H.K., Evans, S.I., Brown, H.M.F., Eberhard, B., Eberhard, N., Kim, M., Moe, H.M., Schaeffer, D., Sharma, R., Thompson, D.W., et al. (2022). Complete Genome Sequences of Six Chi-Like Bacteriophages that Infect *Proteus* and *Klebsiella*. Microbiol. Resour. Announc. 11, e01215211.
- Dunstan, R.A., Pickard, D., Dougan, S., Goulding, D., Cormie, C., Hardy, J., Li, F., Grinter, R., Harcourt, K., Yu, L., et al. (2019). The flagellotropic bacteriophage YSD1 targets Salmonella Typhi with a Chi-like protein tail fibre. Mol. Microbiol. 112, 1831–1846. https://doi.org/10.1111/mmi.14396.
- Kazaks, A., Dislers, A., Lipowsky, G., Nikolajeva, V., and Tars, K. (2012).
 Complete genome sequence of the *Enterobacter cancerogenus* bacterio-phage Enc34. J. Virol. 86, 11403–11404.
- Onmus-Leone, F., Hang, J., Clifford, R.J., Yang, Y., Riley, M.C., Kuschner, R.A., Waterman, P.E., and Lesho, E.P. (2013). Enhanced de novo assembly of high throughput pyrosequencing data using whole genome mapping. PLoS One 8, e61762.
- Lee, J.-H., Shin, H., Choi, Y., and Ryu, S. (2013). Complete genome sequence analysis of bacterial-flagellum-targeting bacteriophage chi. Arch. Virol. 158, 2179–2183.
- Hendrix, R.W., Ko, C.-C., Jacobs-Sera, D., Hatfull, G.F., Erhardt, M., Hughes, K.T., and Casjens, S.R. (2015). Genome sequence of Salmonella phage χ. Genome Announc. 3, e01229-14.
- Hardy, J.M., Dunstan, R.A., Grinter, R., Belousoff, M.J., Wang, J., Pickard, D., Venugopal, H., Dougan, G., Lithgow, T., and Coulibaly, F. (2020). The architecture and stabilisation of flagellotropic tailed bacteriophages. Nat. Commun. 11, 3748. https://doi.org/10.1038/s41467-020-17505-w.
- Wang, C., Duan, J., Gu, Z., Ge, X., Zeng, J., and Wang, J. (2023).
 Architecture of the bacteriophage lambda tail. Structure 32, 35–46.e3.
- Linares, R., Arnaud, C.-A., Effantin, G., Darnault, C., Epalle, N.H., Boeri Erba, E., Schoehn, G., and Breyton, C. (2023). Structural basis of bacteriophage T5 infection trigger and *E. coli* cell wall perforation. Sci. Adv. 9, eade9674.
- Ayala, R., Moiseenko, A.V., Chen, T.-H., Kulikov, E.E., Golomidova, A.K., Orekhov, P.S., Street, M.A., Sokolova, O.S., Letarov, A.V., and Wolf, M. (2023). Nearly complete structure of bacteriophage DT57C reveals architecture of head-to-tail interface and lateral tail fibers. Nat. Commun. 14, 8205.
- Wang, Z., Fokine, A., Guo, X., Jiang, W., Rossmann, M.G., Kuhn, R.J., Luo, Z.-H., and Klose, T. (2023). Structure of *Vibrio* phage XM1, a simple contractile DNA injection machine. Viruses 15, 1673.
- 24. Sonani, R.R., Esteves, N.C., Horton, A.A., Kelly, R.J., Sebastian, A.L., Wang, F., Kreutzberger, M.A.B., Leiman, P.G., Scharf, B.E., and Egelman, E.H. (2023). Neck and capsid architecture of the robust *Agrobacterium* phage Milano. Commun. Biol. 6, 921.
- Fang, Q., Tang, W.-C., Tao, P., Mahalingam, M., Fokine, A., Rossmann, M.G., and Rao, V.B. (2020). Structural morphing in a symmetry-mismatched viral vertex. Nat. Commun. 11, 1–11.
- Orlov, I., Roche, S., Brasilès, S., Lukoyanova, N., Vaney, M.-C., Tavares, P., and Orlova, E.V. (2022). CryoEM structure and assembly mechanism of a bacterial virus genome gatekeeper. Nat. Commun. 13, 7283.

- 27. Huang, Y., Sun, H., Wei, S., Cai, L., Liu, L., Jiang, Y., Xin, J., Chen, Z., Que, Y., Kong, Z., et al. (2023). Structure and proposed DNA delivery mechanism of a marine roseophage. Nat. Commun. 14, 3609.
- 28. Tang, J., Lander, G.C., Olia, A.S., Li, R., Casjens, S., Prevelige, P., Cingolani, G., Baker, T.S., and Johnson, J.E. (2011). Peering down the barrel of a bacteriophage portal: the genome packaging and release valve in p22. Structure 19, 496–502.
- 29. Bárdy, P., Füzik, T., Hrebík, D., Pantůček, R., Thomas Beatty, J., and Plevka, P. (2020). Structure and mechanism of DNA delivery of a gene transfer agent. Nat. Commun. 11, 3034.
- Linares, R., Arnaud, C.-A., Degroux, S., Schoehn, G., and Breyton, C. (2020). Structure, function and assembly of the long, flexible tail of siphophages. Curr. Opin. Virol. 45, 34–42.
- Kizziah, J.L., Manning, K.A., Dearborn, A.D., and Dokland, T. (2020).
 Structure of the host cell recognition and penetration machinery of a Staphylococcus aureus bacteriophage. PLoS Pathog. 16, e1008314. https://doi.org/10.1371/journal.ppat.1008314.
- Rohou, A., and Grigorieff, N. (2015). CTFFIND4: Fast and accurate defocus estimation from electron micrographs. J. Struct. Biol. 192, 216–221. https://doi.org/10.1016/j.jsb.2015.08.008.
- Zheng, W., Wang, F., Taylor, N.M.I., Guerrero-Ferreira, R.C., Leiman, P.G., and Egelman, E.H. (2017). Refined Cryo-EM Structure of the T4 Tail Tube: Exploring the Lowest Dose Limit. Structure 25, 1436–1441.e2. https://doi. org/10.1016/j.str.2017.06.017.
- Punjani, A., Rubinstein, J.L., Fleet, D.J., and Brubaker, M.A. (2017). cryoSPARC: algorithms for rapid unsupervised cryo-EM structure determination. Nat. Methods 14, 290–296. https://doi.org/10.1038/ nmeth.4169.
- Goddard, T.D., Huang, C.C., Meng, E.C., Pettersen, E.F., Couch, G.S., Morris, J.H., and Ferrin, T.E. (2018). UCSF ChimeraX: Meeting modern challenges in visualization and analysis. Protein Sci. 27, 14–25. https:// doi.org/10.1002/pro.3235.
- He, J., Li, T., and Huang, S.-Y. (2023). Improvement of cryo-EM maps by simultaneous local and non-local deep learning. Nat. Commun. 14, 3217.
- Jumper, J., Evans, R., Pritzel, A., Green, T., Figurnov, M., Ronneberger, O., Tunyasuvunakool, K., Bates, R., Žídek, A., Potapenko, A., et al. (2021). Highly accurate protein structure prediction with AlphaFold. Nature 596, 583–589.
- Mirdita, M., Schütze, K., Moriwaki, Y., Heo, L., Ovchinnikov, S., and Steinegger, M. (2022). ColabFold: making protein folding accessible to all. Nat. Methods 19, 679–682. https://doi.org/10.1038/s41592-022-01488-1.
- Emsley, P., and Cowtan, K. (2004). Coot: model-building tools for molecular graphics. Acta Crystallogr. D Biol. Crystallogr. 60, 2126–2132. https://doi.org/10.1107/S0907444904019158.
- Croll, T.I. (2018). ISOLDE: a physically realistic environment for model building into low-resolution electron-density maps. Acta Crystallogr. D Struct. Biol. 74, 519–530.
- Afonine, P.V., Poon, B.K., Read, R.J., Sobolev, O.V., Terwilliger, T.C., Urzhumtsev, A., and Adams, P.D. (2018). Real-space refinement in PHENIX for cryo-EM and crystallography. Acta Crystallogr. D Struct. Biol. 74, 531–544. https://doi.org/10.1107/S2059798318006551.
- van Kempen, M., Kim, S.S., Tumescheit, C., Mirdita, M., Lee, J., Gilchrist, C.L.M., Söding, J., and Steinegger, M. (2023). Fast and accurate protein structure search with Foldseek. Nat. Biotechnol. 42, 243–246.
- Holm, L. (2020). DALI and the persistence of protein shape. Protein Sci. 29, 128–140.
- Krissinel, E., and Henrick, K. (2007). Protein interfaces, surfaces and assemblies service PISA at European Bioinformatics Institute. J. Mol. Biol. 372, 774–797.

Please cite this article in press as: Sonani et al., Cryo-EM structure of flagellotropic bacteriophage Chi, Structure (2024), https://doi.org/10.1016/j.str.2024.03.011

Structure

Article



STAR*METHODS

KEY RESOURCES TABLE

REAGENT or RESOURCE	SOURCE	IDENTIFIER	
Bacterial and virus strains			
S. <i>enterica</i> serotype Typhimurium 14028s	Michael McClelland Laboratory, University of California Irvine School of Medicine, CA, USA	NCBI:txid588858	
Bacteriophage χ (Synonyms: Chivirus chi, Salmonella virus Chi)	Saeed Tavazoie Laboratory, Columbia University, NY 10027, USA	NCBI:txid1541887	
Chemicals, peptides, and recombinant protei	ns		
LB broth	Thermo-Fisher Scientific	Cat #: R453642	
Bacto tryptone	Gibco	CAS #: 91079-40-2	
Yeast Extract	Sigma-Aldrich	CAS. #: 8013-01-2	
Sodium Chloride (NaCl)	Fisher Scientific	CAS. #: 7647-14-5	
Deposited data			
Phage χ capsid structure map	This paper	EMDB-43282	
Phage χ tail structure map	This paper	EMDB-43278	
Phage χ neck structure map	This paper	EMDB-43243	
Phage χ tail tip structure map	This paper	EMDB-43281	
Phage χ capsid structure model	This paper	PDB-8VJI	
Phage χ tail structure model	This paper	PDB-8VJA	
Phage χ neck structure model	This paper	PDB-8VHX	
Phage χ tail tip structure model	This paper	PDB-8VJH	
Software and algorithms			
cryoSPARC	Punjani et al. ³⁴	https://cryosparc.com	
DALI	Holm ⁴³	http://ekhidna2.biocenter.helsinki.fi/dali/	
ChimeraX	Goddard et al. ³⁵	https://www.cgl.ucsf.edu/chimerax/	
PISA	Krissinel ⁴⁴	https://www.ebi.ac.uk/pdbe/pisa/	
Foldseek	van Kempen et al.42	https://search.foldseek.com/search	
Coot	Emsley et al. ³⁹	https://www2.mrc-lmb.cam.ac.uk/ personal/pemsley/coot	
ISOLDE	Croll ⁴⁰	https://tristanic.github.io/isolde/	
AlphaFold2	Mirdita et al. ³⁸	https://colab.research.google.com/	
PHENIX	Afonine et al.41	https://phenix-online.org	

RESOURCE AVAILABILITY

Lead contact

Further information and requests for resources and reagents should be directed to and will be fulfilled by the lead contact, Edward H. Egelman (egelman@virginia.edu).

Materials availability

This study did not generate new unique reagents.

Data and code availability

- All atomic models and density maps from this study are available at the Protein Data Bank (PDB ids: 8VHX, 8VJH, 8VJA and 8VJI) and Electron Microscopy DataBank (EMDB ids: EMD-43243, EMD-43281, EMD-43278 and EMD-43282), respectively.
- No original code is generated in this paper.
- Any additional information required to reanalyze the data reported in this paper is available from the lead contact upon request.

Please cite this article in press as: Sonani et al., Cryo-EM structure of flagellotropic bacteriophage Chi, Structure (2024), https://doi.org/10.1016/j.str.2024.03.011





EXPERIMENTAL MODEL AND STUDY PARTICIPANT DETAILS

Growth conditions for bacteria and phage χ

Bacteriophage χ was propagated on *S. enterica* serotype Typhimurium 14028s using an overlay plate method. *S. enterica* serotype Typhimurium 14028s was grown in LB broth (10 g/l Bacto tryptone, 5 g/l yeast extract, 5 g/l NaCl) at 37°C.

METHOD DETAILS

Cultivation and purification of χ particles

S. enterica serotype Typhimurium 14028s was grown in LB broth (10 g/l Bacto tryptone, 5 g/l yeast extract, 5 g/l NaCl) shaking vigorously at 37°C to an OD600 of approximately 1.0. Motility was verified by phase contrast microscopy. Next, 100 µl of motile culture was combined with approximately 10⁶ plaque forming units of bacteriophage χ. After a 5-minute incubation at room temperature, 4 ml of molten 0.35% LB soft agar was added to the culture-phage mixture, which was immediately poured onto an LB 1.5% agar plate. This procedure was repeated for a total of 60 plates, which were then incubated at 37°C overnight until lysis was visible on the plates. Next, 5 ml of TM buffer (50 mM Tris pH 7.4 and 10 mM MgSO₄) was gently pipetted onto each plate. Plates were placed face-up on a rotating platform at 4°C overnight, rotating slowly at 60 RPM. Liquid containing buffer and loose soft agar from all plates was pooled together in a 250 ml centrifuge bottle and combined with agar lawns that were scraped into the bottle. After the addition of approximately 1 ml chloroform, the agar/buffer mixture was shaken vigorously for one minute to liberate phage particles. The mixture was centrifuged at 10,000 x g for 30 minutes at 4°C, then the supernatant was carefully pipetted into a 250 ml flask. To precipitate phage, NaCl and poly(ethylene glycol) 8000 were added to the lysate to a final concentration of 1 M and 10% (w/v), respectively. The precipitating lysate was mixed on a magnetic stir plate with gentle rotation for 24 hours at 4°C. The precipitated lysate was centrifuged at 15,000 x g for 30 minutes at 4°C, and the supernatant was discarded. The phage-containing pellet was suspended in 2 ml of cold TM buffer. A two-step CsCl density gradient was prepared in disposable ultracentrifuge tubes by gently layering 2 ml of CsCl solution with a density of 1.381 g/ml on top of a 2 ml layer of 1.666 g/ml CsCl solution. The phage lysate was then layered carefully on top of the density gradient and centrifuged at 110,000 x g in a Beckman Coulter Optima™ L-90K ultracentrifuge for 16 hours at 15°C using the SW55Ti swinging bucket ultracentrifuge rotor (Beckman Coulter, USA). After centrifugation, a cloudy blue band appeared within the density gradient, which was extracted using a syringe and 18-gauge needle, transferred to a 10,000 MWCO Thermo Scientific Slide-A-Lyzer® dialysis cassette, and dialyzed against TM buffer for three days at 4°C, changing the buffer once per day. Purified phage was extracted from the cassette and titered via plaque assay.

Cryo-electron microscopy

Data collection and image preprocessing

A 3 μ L volume containing 3.5 \times 10¹² pfu/ml phages was applied onto glow-discharged holey C-flat carbon grids (1.2/1.3, 400 mesh, copper), blotted from the back side, and subsequently subjected to rapid freezing using an EM GP Plunge Freezer (Leica). Cryo-EM data set of a total of 7,510 movies was collected on a 300 keV Titan Krios equipped with a K3 camera (University of Virginia). The pixel size was 0.82 Å with a cumulative electron dose of \sim 50 e Å⁻². The acquired movies underwent correction for motion by 'path motion correction' and the contrast transfer function (CTF) was determined using the 'patch CTF estimation' tools in cryoSPARC. ^{32–34}

Reconstruction

3D reconstructions of capsid, neck and tail tip were achieved by single particle analysis (SPA), whereas the helical reconstruction approach was used for tail reconstruction in cryoSPARC.³⁴ Particles were first selected manually to generate the initial template by 'manual picker'. The generated templates were used for automatic particle picking by 'Template picker' for capsid, neck and tail-tip, and by 'Filament Tracer' for the tail. The picked particles were 2D classified and classes with bad particles were removed. Initial volume for capsid, neck and tail tip were generated by 'Ab initio reconstruction' and further refined by iterative cycles of 'Homogeneous refinement', 'Non uniform refinement', 'Local refinement' and 'Local CTF refinement' as needed.

The initial volume of the capsid was generated by imposing icosahedral symmetry (I) and using a single Ab initio class in the cryoSPARC *Ab-initio reconstruction* job. The initial volume was further refined by maintaining icosahedral symmetry in cryoSPARC's *Homogenous Refinement* job. The resulting high-resolution volume was then utilized for local CTF refinement of individual particles in cryoSPARC. Particles with refined CTF parameters were employed for the final icosahedral averaged reconstruction of the capsid using *Homogenous Refinement* job.

For neck, the initial volume was obtained, refined and used for the refinement of per particle CTF parameters in the similar manner to that was used for the capsid, but by imposing the C6 point group symmetry. The final C6-fold map of neck was reconstructed using the *Non-uniform Refinement'* job of cryoSPARC.

For tail tip, the initial volume was generated by no symmetry imposed and using a single Ab initio class in the cryoSPARC *Ab-initio reconstruction* job. The initial volume was further refined by imposing C3 symmetry in cryoSPARC's *Homogenous Refinement* job. Local mask surrounding the tail tip was generated by ChimeraX, and used for the focused refinement around the tail tip region by *Local refinement* job in cryoSAPRC. Locally refined map was used for the refinement of CTF parameters of the particles which were further used for the final reconstruction of C3-fold map of tail tip in *Local refinement* job. The map of tail-tip was further sharpened by EMReady.³⁶

Please cite this article in press as: Sonani et al., Cryo-EM structure of flagellotropic bacteriophage Chi, Structure (2024), https://doi.org/10.1016/j.str.2024.03.011

Structure Article



For the tail, the averaged power spectrum of vertically aligned tail segments was generated by *Average Power Spetra* job in cryoSPARC. Initial symmetry parameters were calculared by the manual indexing of the power spectrum. The initial volume of tail was generated and refined by imposing the helical symmetry parameters in the *Helix Refine* job. The refined map was used for the refinement of CTF parameters of tail segments in *Local CTF refinement* job, which were subsequestly used for the final reconstruction of the tail using *Helix Refine*. The reconstruction details are provided in Table 2. The map-to-map FSC correlation curves for all reconstructions are depicted in Figure S5.

Model building

AlphaFold³⁷ on the ColabFold server³⁸ was employed to predict all the structure of all 75 proteins of χ . Manual fitting of the predicted protein structures into 3D maps corresponding to the capsid, neck, tail, and tail tip was conducted. Upon identification of a protein component within the map, the fitted AlphaFold model underwent refinement against the density map through iterative cycles of interactive refinement in Coot³⁹ and ISOLDE, ⁴⁰ and real-space refinement using PHENIX. ⁴¹ This process identified a total of 12 proteins. The density for BH2P residues 771–1296 and TMP residue 1–1399 remained unresolved. Detailed statistics of the model-building process are provided in Table 2.

Structural analysis

All structures were analyzed and displayed by ChimeraX.³⁵ Foldseek⁴² and DALI⁴³ were used for structural similarity analysis. PISA⁴⁴ was used to calculate the protein-protein interface area.

QUANTIFICATION AND STATISTICAL ANALYSIS

The quantification and statistical analyses are integral parts of the software (cryoSPARC, DALI, chimeraX, PISA, Foldseek, Coot, ISOLDE, AlphaFold2 and PHENIX) used in the data analysis. Cryo-EM data collection and refinement statistics are provided in Table 2.